Article

Lateral Resolution of a Commercial Optical Coherence Tomography Instrument

Richard F. Spaide[1], Tilman Otto[2], Sophie Caujolle[2], Johannes Kübler[2], Silke Aumann[2], Joerg Fischer[2], Charles Reisman[2], Hendrik Spahr[3], and Annette Lessmann[3]

[1] Vitreous Retina, Macula Consultants of New York, New York, New York, USA
[2] Heidelberg Engineering GmbH, Heidelberg, Germany
[3] Institut Für Biomedizinische Optik, Lübeck, Germany

Correspondence: Richard F. Spaide, Vitreous, Retina, Macula Consultants of New York, 950 Third Ave, New York, NY 10022, USA. e-mail: rickspaide@gmail.com

Purpose: The lateral resolution of an optical coherence tomography (OCT) instrument was considered to be equal to the illumination spot size on the retina. To evaluate the potential lateral resolution of the Spectralis OCT, an instrument calculated to have a 14 µm resolution.

Methods: The lateral point spread function (PSF) was evaluated using diamond abrasive powder 0 to 1 µm in diameter in silicone elastomer and a validated target with 800 nm FeO particles in urethane. The amplitude transfer function was calculated from human OCT images. Finally, resolution was measured using the 1951 USAF target.

Results: Measurement of the lateral PSF from 1215 diamond particle images yielded a full-width half maximum (FWHM) to be 5.11 µm and for 732 FeO particles, 4.9 µm. From the amplitude transfer function, the FWHM of the diffraction limited PSF was calculated to be 5.0 µm. The USAF target imaging showed a lateral resolution of 4.6 µm.

Conclusions: Although a calculation of the spot size of the illumination beam was reported in the past as the lateral resolution of the OCT instrument, the actual lateral resolution is better by a factor of at least 2.5 times. The clinically used A-scan spacing was derived from the calculated, and not the true resolution, and results in under sampling. This set of findings likely apply to all commercial clinical instruments.

Translational Relevance: The scan density parameters of past and present commercial OCT instruments were based on earlier translational concepts, which now appear to have been incorrect.

Introduction

In optical coherence tomography (OCT) imaging, there are two roughly independent factors in resolution, axial and lateral. For any given medium, the axial point spread function (PSF) is a function of the center wavelength and the bandwidth of the light source, the full width half maximum of which is used to calculate the coherence length of the light. For any given medium, the lateral resolution can be estimated from the wavelength used, numerical aperture of the optical system, and the resolution criterion used.[1,2] When light passes through an aperture and is focused by a lens to a bright region centrally surrounded by concentric rings of decreasing intensity. The central bright spot is called an Airy disc. The diameter of the Airy disc can be estimated as:

$$d_{Airy} = \frac{1.22\,\lambda}{NA} \tag{1}$$

with the wavelength λ and the numerical aperture NA which can be approximated by:

$$NA = \frac{d}{2\,f} \tag{2}$$

with the pupil diameter d and the focal length f in air. Past publications stated the lateral resolution of OCT was the same as the spot size on the retina.[1,3–9]

OCT instruments typically use light emitted from a single mode fiber and, as such, the beam profile can be described by Gaussian optics. The beam diameter in the anterior segment for commercial OCT instruments, including the Heidelberg Spectralis, usually is smaller than the pupil and so is only marginally affected by diffraction. The lateral resolution can then be defined by the full-width half maximum (FWHM) of the Gaussian PSF, which is somewhat smaller than the resolution calculated with the Rayleigh criterion. The lateral Gaussian intensity distribution in the focus can be described by:

$$I(r) \propto \exp\left[-\frac{2r^2}{\omega_0^2}\right] \tag{3}$$

with the distance from the axis r, and the beam waist radius ω_0 which is defined as the radius where the intensity falls to $1/e^2$ of their axial value and can be estimated as:

$$\omega_0 = \frac{\lambda}{\pi\ NA} \tag{4}$$

From the beam waist radius, the FWHM can be calculated as[10]:

$$FWHM = \omega_0\sqrt{2\ ln(2)} \tag{5}$$

The return path from the eye follows the same pathway into the single mode fiber on its way to the spectrometer. For a single mode fiber-based system, the setup can be considered confocal, and the resolution is not only described by the size of the illumination spot in the retina. The same PSF that describes the illumination plane also describes the observation plane, so the confocal PSF is the product of the two functions[11] and can be described by:

$$I_{conf}(r) \propto \exp\left[-\frac{4r^2}{\omega_0^2}\right] = \exp\left[-\frac{2r^2}{\left(\frac{\omega_0}{\sqrt{2}}\right)^2}\right] \tag{6}$$

The resolution of a confocal system is related to the PSF of the illuminating and detection systems. From Equation 6, one can derive that the radius where the intensity falls to $1/e^2$ is reduced by $1/\sqrt{2}$ and the confocal lateral resolution in the focus can be calculated as[12]

$$FWHM_{conf} = \omega_0\sqrt{\ln(2)} \tag{7}$$

The amount of potential improvement depends on the beam characteristics. Although light delivered by a single mode fiber has a Gaussian intensity profile, the subsequent optics in the system have a finite size and have the potential to truncate the beam. The greater the truncation, the more of the edges of the illumination profile are blocked by the optical system, leaving the central more uniformly illuminated region to illuminate the sample. The more uniform the illumination, the more the Airy character predominates. For coherent detection, the phase of the light from point scatterers may be variable, making the superposition results difficult to predict. The actual lateral resolving capability of OCT instruments is likely to be better than just the illumination spot size on the retina, but the magnitude of improvement is undefined.

Therefore, because of the uncertainty of what the lateral resolution of an OCT system is, a series of measurements was made. The lateral PSF was evaluated by imaging diamond powder abrasive and a calibrated target of FeO particles. The systems beam intensity profile was measured to estimate the theoretical resolution limits according to the equations above and as an input for a physical optics OpticStudio 21.1.2 (Zemax LLC, Kirkland, WA, USA) simulation. The diffraction limited resolution of the instrument was derived from the complex optical transfer function (OTF) of the OCT image output. In addition, the 1951 USAF target was used to obtain an estimate of lateral resolution, mostly because it has been used in earlier papers.[13–20]

Methods

The Heidelberg Spectralis (Heidelberg Engineering GmbH, Heidelberg, Germany) is a spectral domain OCT device capable of an A-scan rate of 85 kHz while sampling a depth of 1.9 mm. The densest B-scan of the Heidelberg Spectralis has an interscan spacing of 6 μm, which due to the Nyquist sampling theory, would not provide an adequate estimation of the PSF if it were less than 12 μm wide. The scanning pattern was changed through reprogramming to scan every 1.9 μm in the fast axis by using 1536 A-scans in a 10-degree scan. All imaging was done with a high-resolution device based on the Spectralis platform that uses a central wavelength of 853 nm and a bandwidth of 137 nm, yielding an axial resolution of 3 μm in tissue. Where mentioned, the imaging was also duplicated with a conventional Spectralis using a center wavelength of 880 nm and a bandwidth of 40 nm. The imaging evaluations adhered to the tenets of the Declaration of Helsinki and the imaging protocol was approved by the Western Institutional Review Board.
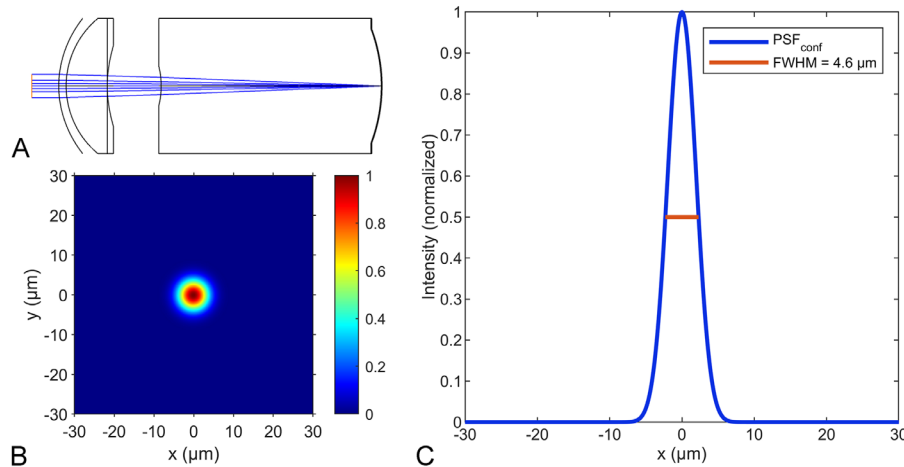
Figure 1. OpticStudio modeling of the eye. (**A**) A Navarro eye model was used with light having a central wavelength of 853 nm. (**B**) The graphical representation of the light spot produced on axis at the level of the retina. (**C**) The plot of the confocal intensity versus the displacement from the center of the beam shows a full width half maximum of 4.60 ± 0.02 µm.

Diamond Powder and Calibrated FeO Particle Imaging

The first estimates of the lateral PSF were derived from diamond powder with a diameter of 0 to 1 µm suspended in clear silicone elastomer. An estimation of the lateral PSF of less than 6 µm was calculated. To obtain a more precise measurement, a validated target (National Physical Laboratory, Teddington, Middlesex, UK) using FeO particle <800 nm suspended in polyurethane was imaged.[12] Both experiments were conducted by focusing the beam using an additional lens with a focal length of 40.18 mm. This lens was chosen to avoid the problems of using a shorter focal length lens in air, such as field curvature, spherical aberration, and a restricted Rayleigh length. An external software tool was used to evaluate the linear OCT signal without any signal processing. The signal is represented by a 32-bit value ranging from 0 to 1. Three separate B-scans within a volume were evaluated. The software tool evaluated the image for reflectivity peaks below 0.99 and above 0.5 within a 2D circular neighborhood with a diameter of 13 pixels. Because the depth of the test sample was within the Rayleigh length of the OCT system, the full depth of point samples was used. The horizontal signal profile was then extracted, and the distributions were aligned by shifting the center of mass of the distribution at a 0.1 sub-pixel resolution. The profiles were then measured, and the standard deviation was calculated. Profiles greater than three standard deviations from the mean were excluded, to reduce the likelihood that particle aggregates would influence the results. The distributions were normalized so the peaks would be equal to one and then averaged.

Measurement of OCT Beam Characteristics

The collimated beam diameter of the OCT system was measured at the location where the pupil of the eye is typically located using an infra-red camera (Allied Vision Technologies Pike F-032B, Germany).

OpticStudio Simulation

A physical optics simulation for a Gaussian beam was performed using OpticStudio. The simulation model comprises a Gaussian source with a $1/e^2$ diameter of 1.71 mm as measured after the objective of the Spectralis system entering a Navarro eye model,[21] and a central wavelength of 853 nm (Figs. 1A and B).

Amplitude Transfer Function

The achievable resolution is limited by diffraction, which is mainly given by the beam diameter of the instrument, and aberrations in the entire optical system, which are dominated by ocular contributions. The resolution that can be achieved in the human eye is therefore patient-specific and it is not possible to determine a universally valid value. However, a fundamental diffraction limit can be determined, which cannot be exceeded even in the complete absence of ocular aberrations.

So far, we have determined this upper limit using artificial eye models and technical samples. Now, we validate it by ocular examinations for three healthy subjects using the Heidelberg Spectralis and the High Resolution Spectralis instruments. For this purpose, the spatial frequencies contained in the OCT images
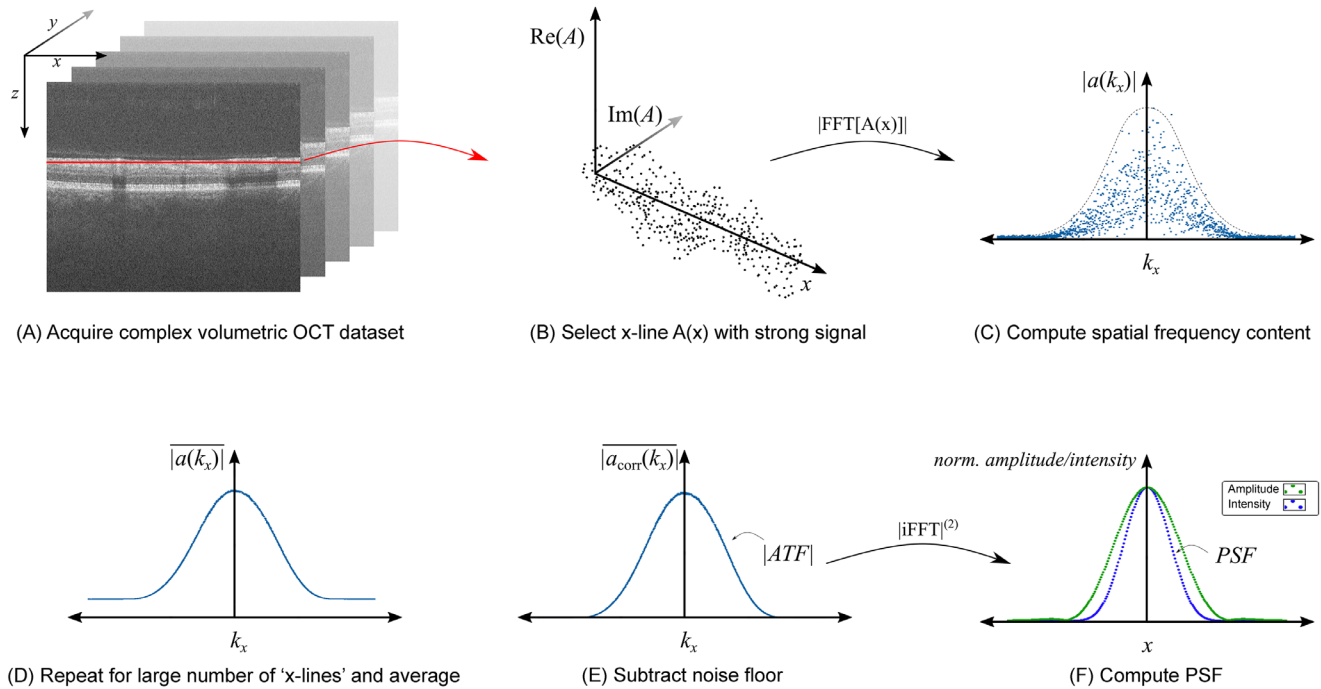
Figure 2. Illustration of the Fourier analysis for a determination of the diffraction limited point spread function (PSF). (**A**) A sufficiently large, complex OCT dataset is recorded. The motion induced phase shift between adjacent A-scans is corrected. (**B**) A horizontal line of a B-scan (i.e. a line running at constant depth along the fast scan direction x), is selected (this will be referred to as an "x-line"). (**C**) By a Fourier transformation and subsequent calculation of the magnitudes, the spatial frequency spectrum of this line is determined. It contains the spatial frequencies originally present in the object plane carrying the image information multiplied by the amplitude transfer function (ATF). (**D**) By repeating these steps for a very large number of different (and uncorrelated) "x-lines" and averaging, the shape of the ATF can be estimated. (**E**) To increase accuracy, the noise floor is subtracted. It is determined from "x-lines" that contain no signal, but only noise. (**F**) By means of an inverse Fourier transform, the PSF of the amplitudes can be determined. Finally, by squaring, the PSF of the intensities is obtained. The calculated FWHM of the diffraction limited PSF was 4.98 μm in the eye.

are analyzed, because they are not changed by aberrations (i.e. the speckle present in OCT images are always as small as the diffraction limits allows).[22] We assume that the retina has a fine microstructure that exceeds the resolution of the optics of the Spectralis. This means that the spatial frequency spectrum in the object plane is broad, and only a small fraction of these spatial frequencies is transmitted by the imaging optics to the image plane, where they contribute to the formation of the OCT image.[23] Which spatial frequencies are transferred, and to what extent, is described by the magnitude of the amplitude transfer function (ATF).[22] The phase of the ATF indicates how various frequency components of the image are shifted in respect to each other, leading to distortion and blurring as the result of aberrations. Whereas often the phases of the ATF are of interest to characterize or correct aberrations,[24–30] we focus on the magnitudes, because they determine the maximum resolution achievable in the diffraction limit.[22] The Fourier transform of the magnitude of the ATF represents the diffraction limited PSF. To estimate it, we first determine the

spatial frequency spectrum of iso-depth lines along the fast scan axis x (i.e. horizontal lines within a B-scan for constant y and z). For this analysis, we consider the originally detected complex amplitudes after correcting axial motion between adjacent A-scans. The lines in which the overall signal strength exceeded the 99th percentile were selected for computation of the Fourier magnitudes, and averaged to obtain the profile of the ATF. All lines with an overall signal below the first percentile were used to estimate and remove the noise floor. The inverse Fourier transform of the ATF magnitudes yields the profile of the diffraction limited PSF, whose FWHM we determined subsequently. A graphical representation of the steps is shown in Figure 2.

1951 USAF Target

A USAF target (R1DS1N, Thorlabs) was imaged by focusing the beam using an additional lens with a focal length of 40.18 mm. The resultant images were rescaled for retina measurements using the focal length of an emmetropic eye, f = 16.7 mm. For each acquisition,

the focus was adjusted to obtain the sharpest image. The contrast of the different elements of the USAF target was calculated on the B-scan images by dividing the mean difference in reflective background surface the foreground and background grayscale values by the foreground grayscale values reflective background surface. The USAF target evaluated resolution directly and not the FWHM of the PSF.

Retinal Imaging

Healthy subjects were imaged with 1.9 and 6 μm A-scan spacing with both the Spectralis, which has an axial resolution of 7 μm and a high-resolution version of the Spectralis with 3 μm axial resolution in tissue.

Results

Diamond Powder and FeO Particles

The lateral image measurement of the diamond powder and the calibrated target is expected to be the convolution of the instrument PSF and the object. The particles within 3 B-scan images of the diamond powder were evaluated and within the 3 B-scans, 462, 454, and 299 profiles were averaged (Fig. 3). The weighted average of these three curves revealed a FWHM of 5.11 ± 0.034 μm in the eye. The FeO suspended in polyurethane was evaluated in 3 B-scans with 196, 249, and 287 points in these B-scans. The weighted average of the FWHM of the PSF for the FeO particles was 4.9 ± 0.033 μm. Because this measurement was much greater than the particle size, the measured PSF is roughly equal to the instrument PSF.

Beam Characteristics

The beam appeared to be radially symmetric and therefore was radially averaged and multiple measurements were averaged. The mean beam profile had a Gaussian distribution, and the $1/e^2$ beam diameter was calculated to be 1.71 ± 0.01 mm. There were minor deviations from the Gaussian fit near the centroid of the beam and again toward the outer edge of the distribution as shown in Figure 4.

OpticStudio Simulation

The simulation results in a 2D illumination profile in the retina as depicted in Figure 3. With Equation 7 the theoretical diffraction limited confocal lateral
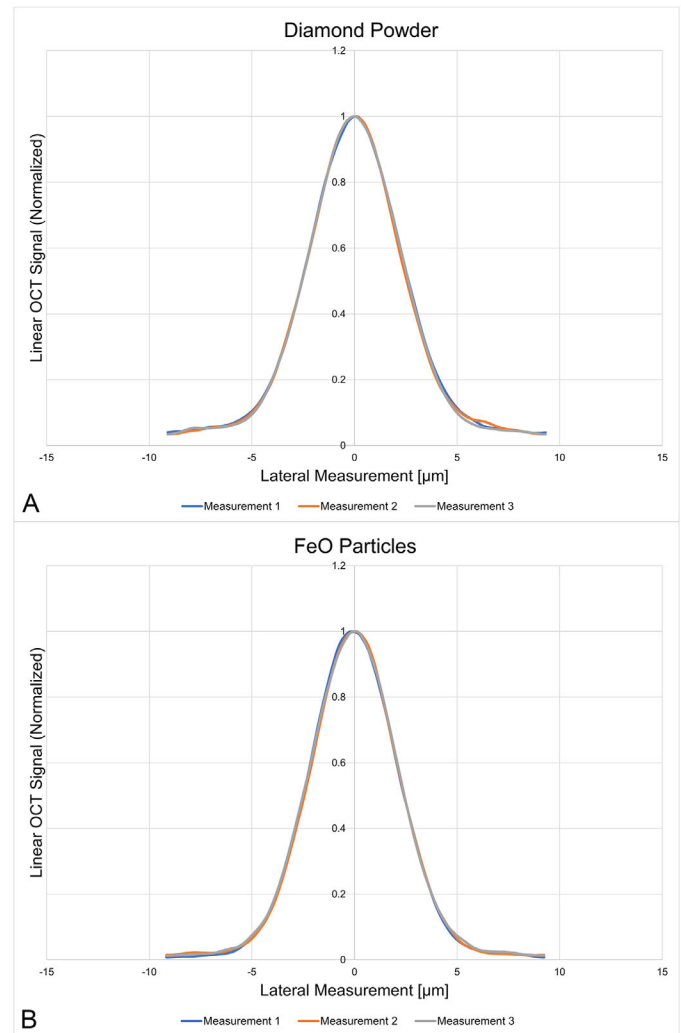

Figure 3. Lateral point spread function estimates from measuring small particles. (**A**) The plots of measurements obtained from 3 different B-scans of 0 to 1 μm diamond powder abrasive suspended in silicone elastomer. (**B**) The plots of measurements obtained from 3 different B-scans of 800 nm FeO particles. The FWHM was 5.11 μm for diamond powder and 4.9 μm for FeO particles.

resolution of the OCT system in the eye is 4.42 μm, assuming a central wavelength of 853 nm, effective focal length of the eye of 16.7 mm, and measured beam diameter of 1.71 mm. The OpticStudio simulation using a Navarro model, including spherical aberrations, provided a FWHM estimate of 4.60 ± 0.02 μm (see Fig. 1C).

Amplitude Transfer Function Evaluation

The mean magnitude of the Fourier transformed iso-depth lines (i.e. the estimated ATF magnitude), is shown in Figure 2. The squared absolute inverse Fourier transform of these values provides an
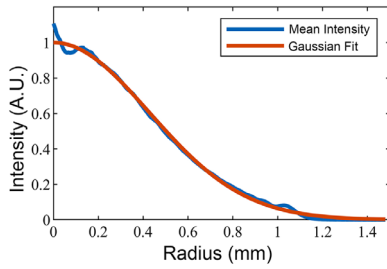
Figure 4. Beam characteristics as measured at the working distance. The beam was imaged with an infrared camera and the beam images were radially averaged. The profile is very close to a Gaussian profile with small fluctuations at either extreme of the x-axis. Near the centroid of the beam very few pixels are averaged, and the measurements appeared to be affected both by the effects of speckle and some subtle diffraction patterns produced by dust or small imperfections in the optics. Toward the outer edge there was some variation that may have been caused by truncation due to an aperture within the optical system.

Table 1. Measured Performance

Test Object	Estimated Lateral Point Spread Function (μm)
0–1 μm diamond powder	5.1
FeO particles (0.8 μm)	4.9
Fourier analysis of the amplitude transfer function[a]	5.0
Diffraction limited performance calculated from the beam characteristics	4.4
OpticStudio simulation	4.6
1951 USAF Target[b]	4.6

[a]Diffraction limited performance,
[b]Resolution, not point spread function.

estimation for the diffraction limited PSF (for intensities), with a FWHM of 4.98 ± 0.06 μm in the eye.

1951 USAF Target

Figure 5 shows the B-scan profiles of element 2, 3, 4, and 5 from group 6 of the USAF target. Elements 2, 3, and 4 had discernable fluctuations with contrast measurements from the peak values of 42%, 29%, and 19%. Reliable fluctuations in the reflectance profile
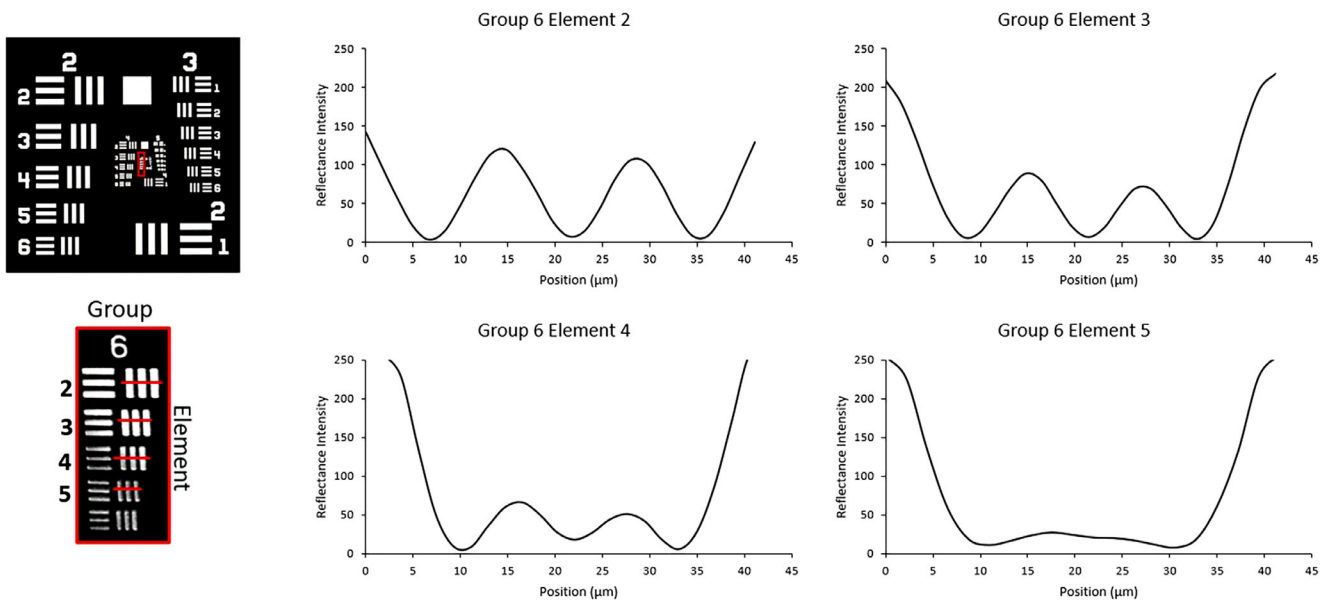
were seen as small as element 4, which corresponds to a lateral resolution of 4.6 μm in the eye.

A summary of the measurements is shown in Table 1.

Retinal Imaging

Comparative retinal imaging obtained with an A-scan separation of 6 μm and 2 μm are shown for the conventional Heidelberg Spectralis with 7 μm axial resolution and a new high-resolution version with 3 μm axial resolution as shown in Figures 6 and 7, respectively.

Figure 5. Reflectance profiles from the USAF target. For the USAF target used, the black lines in this figure were reflective against a transparent background. The increasing spatial frequency of the target was associated with decreasing image contrast. The image contrast decreased from 42%, 29%, and 19% in going from group 6, element 2 to element 3 to element 4. Group 6 element 4 corresponds to a lateral resolution of 4.6 μm in the eye.
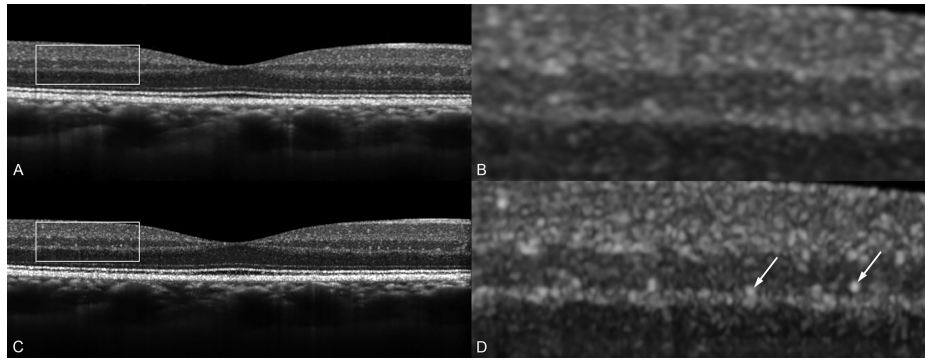
Figure 6. Conventional Heidelberg Spectralis images, which has an axial resolution of 7 µm. (**A**) Image obtained with 6 µm spacing between A-scans, currently the highest density available. The rectangular outline is magnified in (**B**). (**C**) The same subject in a matched location imaged with 1.9 µm A-scan spacing. The enlargement from the rectangular area is shown in (**D**). Note the vascular profiles in the deep capillary plexus show both greater delineation for the tissue because of increased sharpness and contrast (*arrows*).
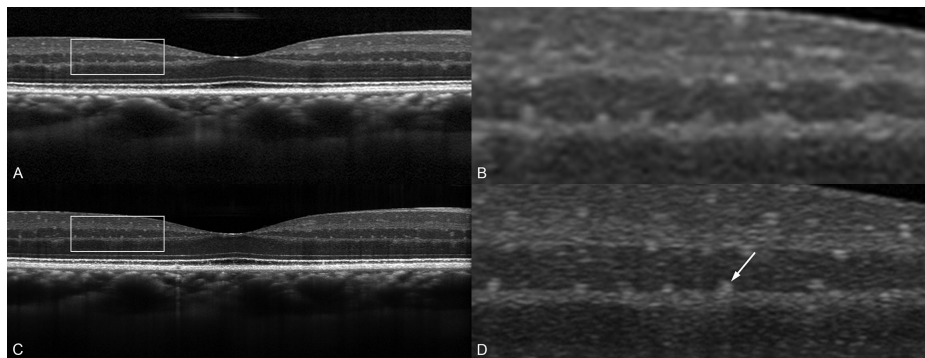

Figure 7. Heidelberg High Resolution Spectralis images, which has an axial resolution of 3 µm. (**A**) Image obtained with 6 µm spacing between A-scans. The rectangular outline is magnified in (**B**). (**C**) The same subject in a matched location imaged with 1.9 µm A-scan spacing. Note vascular shadows can be seen below capillaries in the deep capillary plexus. The enlargement from the rectangular area as shown in (**D**) shows greater sharpness with increased edge delineation (*arrow*).

Discussion

Optical resolution, the ability to detect the presence of two closely spaced points as being physically different from a single point, has many potential definitions. Light emanating from a point in the object space is imaged, not as a point, but as a distribution of light over an area. The PSF describes the characteristic of this spot. One standard for measuring resolution is to consider the image of a point source to be an Airy disk and the limits of resolution to be where the maximum of the Airy disk from one source lies in the first minimum of the diffraction pattern in the Airy disk of another source, and this is known as the Rayleigh criterion. In systems using light originating from a point source, such as OCT or confocal microscopy, the Airy disk may be difficult to measure. Instead, the FWHM of the light distribution is used as

it is relatively easy to measure and represents the lateral PSF of the illumination system. In confocal imaging, there is a radial reduction in the intensity of the illumination and a corresponding radial reduction in the sensitivity of detection. This apodization removes the influences of potential side-lobes in the illumination and detection systems' optical performance and shapes the lateral point spread function of confocal imaging systems. Thus, the PSF of the system, rather than just the spot size on the retina or just the lateral PSF of the detection system, becomes the paramount metric to evaluate lateral resolution produced in the image. The estimates of the lateral PSF of the OCT instrument, the Heidelberg Spectralis, from particles resulted in an estimate of a FWHM of 5.11 µm for diamond powder and 4.9 µm for the FeO target. The Fourier analysis, which estimates the diffraction limited performance, yielded 5.0 µm and the OpticStudio modeling produced the estimate of 4.6 um. These

results are comparable, and each method has its own limitations, as will be discussed below. The USAF target, which has been used to estimate lateral resolution of OCT instruments, showed a lateral resolution of 4.6 µm.

The diamond powder target was prepared by mixing the 0 to 1 µm diamond particles with silicone elastomer before it polymerized. With extensive stirring, the diamond particles are separated to produce individually reflecting grains. It is possible that small aggregates of grains were present in the test sample and imaged as one particle. To avoid inclusion of large aggregates, we limited the analysis to particle signals whose FWHM lies within three standard deviations of the overall mean. The mean PSF subsequently calculated from diamond powder was 4.7% larger than that measured from a validated sample containing FeO particles that were 800 nm in diameter. Possible reasons for the difference include a greater tendency toward clumping with the diamond particles, a larger distribution in the size of the diamond grains, and possible inaccuracies in the size estimation of the diamond grains. The distribution of the intensity of the reflections showed tails of the distribution that were slightly more elevated from zero with the diamond particles than for the FeO particles, suggesting a wider range of particle sizes in the diamond powder sample (see Fig. 3). We did not independently measure the size of the diamond powder grains or the resultant suspended particles. In the sequence in the measurements, the diamond particles were measured first and then a validated test object using FeO was evaluated, which confirmed and potentially refined the measurements made from the diamond particles.

Images derived from human eyes with no pharmacologic dilation were used to determine the magnitudes of the complex ATF. Using this analysis, we calculated the diffraction limited resolution to be approximately 5.0 µm. This is a theoretical value that has an uncertain relationship with actual resolution in the eye, which can have significant aberrations. The relative proportions of diffraction versus aberrations in limiting optical performance are related to pupil sizes. In eyes with smaller pupils, diffraction limits the optical performance, whereas at large pupil sizes, aberrations dominate. Given the $1/e^2$ size of 1.71 mm, diffraction may play a role in the lateral resolution of OCT in clinical practice, particularly in patients with undilated pupils.

The 1951 USAF target was used for estimation of the lateral resolution. This target has two groups of triplets of bars for each resolution arranged orthogonal to each other. We measured the resolution along the fast axis of the scan. The resultant reflectance profiles showed decreasing contrast with increasing spatial frequency, as would be expected. There are differing methods of inferring image resolution; with the Rayleigh criterion the contrast ratio is 26.4%. There is the Sparrow criterion, which is essentially 0% and other criteria for resolution lying in between. Thus, we show the elements in the USAF chart and their corresponding contrast measurements. Because there were easily discernable variations in the brightness in group 6, element 4, but not in element 5, the resolution was calculated to be 4.6 µm in the eye. The USAF target was established for incoherent imaging, and there is a possibility that in a coherent regime there could be destructive or constructive interference produced by reflections from between the dark and light regions. This has the possibility of creating bars with lighter or darker appearance than what they would have been using an incoherent imaging method, and thereby bias the true estimate of image resolution. If the flat surface is scanned with a focused beam, then the local angle of incidence inevitably varies across the target. The mirrored beam is not reflected exactly into itself across much of the target, so that depending on the scan position, only a certain portion of the numerical aperture (NA) is actually used. We include the USAF evaluation here because of its historical use.[13–20]

The various test modalities used in this study all consistently point to a PSF of the instrument being much better than the beam width on the retina, quoted to be 14 µm for the Spectralis. As currently implemented in the commercial instrument, the actual resolution of the instrument was not realized because the tissue sampling was done at an interval to achieve 14 µm lateral resolution, that is, a 6 µm A-scan spacing. The lower resolution expectation was cemented in place by engineering designed to achieve only the lower lateral resolution. To recover the inherent resolution capabilities of the instrument a scan spacing of 1.9 µm was used in the present study. This sampling is slightly more than three times the "High Resolution" mode of the commercially available instrument. The original A-scan rate of the instrument was selected as an optimization among costs at the time, the lateral resolution as it was understood, and convenience for the operator and patient in terms of scan times. Just increasing the scan density by a factor of three through a software modification would not incur significant hardware costs and would help achieve better lateral resolution. In practical use, increasing the scan density would create a much larger burden on the patient, operator, and eye tracking system because of the necessary increase in scanning time and precision

Table 2. Claimed Lateral Resolutions of Commercial Optical Coherence Tomography Instruments

Company	Heidelberg Engineering	Optovue				Topcon		Zeiss	
Instrument	Spectralis OCT	Solix FullRange	Avanti	AngioVue	iVue	DRI OCT Triton Plus	3D OCT-1 Maestro 2	Cirrus 6000	Plex Elite 9000
Claimed Optical Transverse Resolution	14 µm	15 µm	15 µm	15 µm	15 µm	20 µm	20 µm	15 µm	20 µm
References	31	32	33	34	35	36	37	38	39

Company	Nidek			Optos		Optopol	Canon		Huvitz
Instrument	RS-3000 Advance AngioScan	Retina Scan Duo RS-330	Mirante	Monaco	Silverstone	Reno	Xephilio OCT-A1	Xephilio OCT-S1	HOCT-1/1F
Claimed Optical Transverse Resolution	20 µm	20 µm	20 µm	20 µm	20 µm	12 µm (18 typically)	20 µm	30 µm	20 µm
References	40	41	42	43	44	45	46	47	48

required in maintaining image alignment. To realize the true potential lateral resolution with a convenient scanning time, a much higher A-scan rate would be necessary. Tighter tolerances in the slow axis scanning to improve the positioning of the adjacent B-scans would be required as well for an optimal system. Although this study of the disparity between stated spot size on the retina and the actual achievable PSF was measured in the Heidelberg Spectralis, there are reasons to believe these same factors likely apply to every OCT device in the marketplace. It may be possible that all available instruments under sample the tissue. Increasing the A-scan rates of commercial OCT instruments has been a trend for decades, and part of the motivation is to be able to scan increasingly large areas. The increased A-scan rates may also be used to configure scanning protocols that avoid under sampling to improve achievable lateral resolution available in the clinic.

How we image these structures is a function of past translational efforts of converting theoretical theories into clinical practice. The resultant images obtained helped form our current concepts of the retina and choroid in health and disease. The determinants of lateral resolution proposed many years ago, which seemed to have forged currently used scanning parameters, do not appear to be correct. The actual lateral resolution of OCT appears to be much better than previously proposed, with no structural change in the scanner necessary. Part of translational research is the testing longstanding assumptions and by improving resolution may help drive development of improved understanding of retinal physiology and disease in the future. These changes would appear to apply to current commercial OCT instruments by all manufacturers, as their stated lateral resolution is generally between 15 and 25 µm. By the same logic used in our analysis, it is likely the actual lateral resolution of these instruments is potentially much better (Table 2).

Acknowledgments

References

1. Aumann S, Donner S, Fischer J, Müller F. Optical Coherence Tomography (OCT): Principle and Technical Realization. In: *High Resolution Imaging in Microscopy and Ophthalmology*. New York, NY: Springer International Publishing; 2019:59–85.

2. Popescu DP, Choo-Smith LP, Flueraru C, et al. Optical coherence tomography: fundamental principles, instrumental designs and biomedical applications. *Biophysical Rev*. 2011;3(3):155–169.

3. Drexler W. Ultrahigh-resolution optical coherence tomography. *J Biomed Optics*. 2004;9(1):47.

4. Drexler W, Morgner U, Ghanta RK, Kärtner FX, Schuman JS, Fujimoto JG. Ultrahigh-resolution ophthalmic optical coherence tomography. *Nat Med*. 2001;7(4):502–506.

5. Reddikumar M, Tanabe A, Hashimoto N, Cense B. Optical coherence tomography with a 2.8-mm beam diameter and sensorless defocus and astigmatism correction. *J Biomed Optics*. 2017;22(2):026005.

6. Atry F, de La, Rosa IJ, Rarick KR, Pashaie R. Design and Implementation Guidelines for a Modular Spectral-Domain Optical Coherence Tomography Scanner. *Int J Optics*. 2018;2018:1–22.

7. Gramatikov BI. Modern technologies for retinal scanning and imaging: An introduction for the biomedical engineer. *BioMed Eng Online*. 2014;13(1):52.

8. Fujimoto JG. Optical Coherence Tomography: Introduction. In: Bouma BE, Tearney GJ, eds. *Handbook of Optical Coherence Tomography*. New York, NY: Marcel Dekker; 2002:1–40.

9. Cordes AH, Couceiro IB, Alvarenga AD, et al. Practical considerations for OCT applications. *J Physics Conf Series*. 2021;1826(1):012064.

10. Hitzenberger CK. Principles of Optical Coherence Tomography. In: Fankhauser F, Kwasniewska S, eds. *Lasers in Ophthalmology Basic Diagnostic and Surgical Aspects. A Review*. Amsterdam, The Netherlands: Kagler Publications; 2003:61–72.

11. Webb RH. Confocal optical microscopy. *Rep Prog Physics*. 1996;59(3):427–471.

12. Tomlins PH, Ferguson RA, Hart C, Woolliams PD. Point-Spread Function Phantoms for Optical Coherence Tomography. Teddington, Middlesex, UK: National Physical Laboratory; 2009;(August).

13. Hu Z, Hao B, Liu W, Hong B, Li J. Test target for characterizing 3D resolution of optical coherence tomography. In: Czarske J, Zhang S, Sampson D, Wang W, Liao Y, eds. *Proc. SPIE 9297, International Symposium on Optoelectronic Technology and Application 2014: Laser and Optical Measurement Technology; and Fiber Optic Sensors*. 2014;9297:92971S 7.

14. Lee BH, Choi WJ, Na J. Full-Field Optical Coherence Tomography Based on Hilbert Transform. *Rev Laser Eng*. 2008;36(APLS):1347–1350.

15. Marques MJ, Hughes MR, Vyas K, et al. Enface optical coherence tomography/fluorescence endomicroscopy for minimally invasive imaging using a robotic scanner. *J Biomed Optics*. 2019;24(06):1–15.

16. Lichtenegger A, Gesperger J, Niederleithner M, et al. Ex-vivo Alzheimer's disease brain tissue investigation: a multiscale approach using 1060-nm swept source optical coherence tomography for a direct correlation to histology. *Neurophotonics*. 2020;7(3):035004.

17. Tan B, Hosseinaee Z, Han L, Kralj O, Sorbara L, Bizheva K. 250 kHz, 15 μm resolution SD-OCT for in-vivo cellular imaging of the human cornea. *Biomed Optics Express*. 2018;9(12):6569–6583.

18. Chen Y, Trinh LA, Fingler J, Fraser SE. Phase variance optical coherence microscopy for label-free imaging of the developing vasculature in zebrafish embryos. *J Biomed Optics*. 2016;21(12):126022.

19. Du M, Eikema KSE, Witte S. Computational-imaging-based optical coherence tomography in time- and frequency-domain. *OSA Continuum*. 2019;2(11):3141.

20. Israelsen NM, Petersen CR, Barh A, et al. Real-time high-resolution mid-infrared optical coherence tomography. *Light: Science & Applications*. 2019;8(1):11.

21. Navarro R, Santamaría J, Bescós J. Accommodation-dependent model of the human eye with aspherics. *J Opt Soc Am A*. 1985;2(8):1273–1281.

22. Goodman JW. *Introduction to Fourier Optics,* 3rd ed. Englewood, CO: Roberts & Co. Publishers; 2005.

23. Schmitt JM, Xiang SH, Yung KM. Speckle in Optical Coherence Tomography. *J Biomed Optics*. 1999;4(1):95.

24. Stadelmaier A, Massig JH. Compensation of lens aberrations in digital holography. *Optics Letters*. 2000;25(22):1630.

25. Fienup JR, Miller JJ. Aberration correction by maximizing generalized sharpness metrics. *J Opt Soc Am A*. 2003;20(4):609.

26. Ralston TS, Marks DL, Carney PS, Boppart SA. Interferometric synthetic aperture microscopy. *Nat Physics*. 2007;3(2):129–134.

27. Adie SG, Graf BW, Ahmad A, Carney PS, Boppart SA. Computational adaptive optics for broadband optical interferometric tomography of biological tissue. *Proc Natl Acad Sci USA*. 2012;109(19):7175–7180.

28. Adie SG, Shemonski ND, Graf BW, Ahmad A, Scott Carney P, Boppart SA. Guide-star-based computational adaptive optics for broadband interferometric tomography. *Appl Phys Lett*. 2012;101(22):221117.

29. Ahmad A, Shemonski ND, Adie SG, et al. Real-time in vivo computed optical interferometric tomography. *Nat Photonics*. 2013;7(6):444–448.

30. Shemonski ND, South FA, Liu YZ, Adie SG, Carney PS, Boppart SA. Computational high-resolution optical imaging of the living human retina. *Nat Photonics*. 2015;9(7):440–443.